DOI: 10.7860/JCDR/2024/68452.18927

Original Article

Radiology Section

Utility of Multiparametric MRI of the Breast with Combined High b-value DWI and Dynamic Contrast MRI to Differentiate Benign and Malignant Lesions: A Cross-sectional Study

PRATIKSHA YADAV[1], YASHRAJ PATIL[2], SAUMYA HARIT[3]

(cc) BY-NC-ND

ABSTRACT

Introduction: Breast cancer is one of the most frequent malignancies in women worldwide, and it is the leading cause of cancer mortality. Early detection is key to a better prognosis. In India, many patients are diagnosed in later stages due to the absence of screening programs and less awareness in certain regions of the country. MRI is a highly sensitive investigation that can detect small and sometimes hidden or occult lesions not visible on mammography. The diffusion-weighted sequence has the potential to be used in conjunction with mammography, thereby improving diagnostic accuracy.

Aim: To evaluate the utility of multiparametric MRI (mpMRI) of the breast, combining high b-value Diffusion-Weighted Imaging (DWI) and Dynamic Contrast-Enhanced Magnetic Resonance Imaging (DCE-MRI), in differentiation benign and malignant lesions.

Materials and Methods: This cross-sectional study was conducted at a Dr. D.Y. Patil Medical College, Hospital and Research Centre, Pimpri, Pune, India from Jan 2017 - Dec 2020. A total of 254 women with 272 breast lesions were included. All cases underwent mpMRI on a 3Tesla scanner, which included T2-weighted imaging, dynamic post-contrast study, and DWI with a b-value of 1500 sec/mm^2. Sensitivity, specificity, diagnostic accuracy, and area under the curve were calculated using the results of different parameters. Comparative Receiver Operating Characteristic (ROC) curves were plotted for DCE-MRI, DWI, and mpMRI. Histopathologic diagnosis was considered the standard of reference.

Results: The mean age was 43.73±13.56 years, with an age range of 18-82 years. Both benign and malignant breast lesions were most common in the 40-49 years age group, accounting for a total of 80 (31.4%) lesions. Out of the 272 lesions, 141 (52.03%) were malignant and 131 (47.97%) were benign. DCE-MRI showed 97.87% sensitivity, 80.15% specificity, and 89.33% diagnostic accuracy. Diffusion-weighted MRI showed 97.16% sensitivity, 87.02% specificity, and 92.27% diagnostic accuracy. The ROC analysis for Apparent Diffusion Coefficient (ADC) values of the 272 lesions revealed an area under the curve of 0.985 ($p<0.001$) and a sensitivity of 92.91%, with an ADC cut-off of 0.987×10^{-3} mm^2/sec. The multiparametric study demonstrated 98.58% sensitivity, 93.13% specificity, and 95.95% diagnostic accuracy. The area under the curve was 0.959 for mpMRI, 0.921 for DWI, and 0.890 for DCE-MRI.

Conclusion: mpMRI with DCE-MRI and DWI using a high b-value of 1500 sec/mm^2 can be utilised to improve diagnostic accuracy.

Keywords: Beast imaging, Biopsy, Breast cancer, Cancer screening, Diffusion weighted imaging, Early detection

INTRODUCTION

Breast cancer is one of the most frequent malignancies in women worldwide, and it is the leading cause of cancer mortality. The global burden of breast cancer cases is expected to reach about 2 million by the year 2030, with an increasing proportion of cases from developing countries [1].

The American College of Radiology standardised the breast imaging reporting and classification system, known as Breast Imaging Reporting and Data System (BIRADS), for mammography, ultrasound breast, and breast MRI. The 5th edition of the MRI breast BIRADS lexicon provides morphologic and functional descriptors using DCE-MRI characteristics, which help determine the probability of a malignant lesion. DCE-MRI is the most sensitive radiologic investigation for breast cancer. However, distinguishing between benign and malignant breast lesions is sometimes not possible with these methods due to the overlapping morphologic and kinetic features of both types [2,3].

Studies have revealed the utility of DWI in differentiating benign from malignant breast lesions, showing good sensitivity [4-6]. mpMRI, which combines morphologic and various functional MRI parameters such as DCE-MRI, DWI, and MR spectroscopy, has shown improved diagnostic accuracy in some studies [7-9]. Among all the parameters evaluated as adjuncts to DCE-MRI, DWI is the most feasible parameter with practical clinical application. Some studies have demonstrated that MRI Breast using DWI and DCE-MRI significantly improves the diagnostic accuracy of breast MRI [10-14].

The DWI technique based on the readout-segmented echo-planar (RESOLVE) sequence has improved image quality with fewer artifacts and background noise, as well as less distortion, allowing for analysis of small lesions [15]. Semi-quantitative DCE-MRI parameters, along with qualitative and quantitative variables of DWI, have the potential to improve diagnostic accuracy [13,14].

There are a few studies that have evaluated the use of high b-value for better cancer detection [11,16,17]. In most of the previous DWI studies, a b value of 800 was used [7,8,14]. DWI using RESOLVE obtains a high spatial resolution image with fewer artifacts and background signal noise, thereby improving lesion visibility on DWI [15-18]. In this multiparametric model, the present study objective was to evaluate the utility of morphology descriptors, DWI (RESOLVE technique) with a high b value, and DCE-MRI for potential use in increasing the diagnostic accuracy of breast MRI.

MATERIALS AND METHODS

This cross-sectional single institutional study was approved by the Institutional Review Board and Institutional Ethics Committee (Ref. no. DYPV/EC/174/17). The study was conducted at a Tertiary care university hospital, Dr. D.Y. Patil Medical College, Hospital, and Research Centre, Pune, India, from January 2017 to December 2020. Written informed consent was obtained from each patient included in the study, and identity secrecy was maintained throughout.

Sample size calculation: The sample size was calculated based on the sensitivity of the author's pilot study and previous published studies [13,14,19] to achieve a precision of 0.05.

A total of 428 women were enrolled in this prospective study; however, 174 patients with normal MRI and benign findings, as well as patients who were subjected to follow-up for benign lesions and did not undergo biopsy, were excluded from the study.

Inclusion criteria: Those patients (>18 years) with abnormal lesions and/or masses detected on digital mammography and/or breast ultrasound, micro-calcification asymmetry, or architectural distortion detected on digital mammography, female patients with clinically palpable lumps or indeterminate diagnosis on mammography were included in the study.

Exclusion criteria: Pregnant or breastfeeding individuals, previous breast cancer treatment cases, and those with contraindications for MRI or MRI contrast agents , those cases without histopathological confirmation by image-guided or surgical biopsy or excision and the MRI images with severe motion artifact, susceptibility error, etc., were excluded from the study.

Procedure

Full clinical history was obtained from each patient, and a clinical examination was performed. MRI was conducted before biopsy of the breast lesion using a 3Tesla scanner (MAGNETOM Vida, Siemens, Germany) with a dedicated 18-channel breast coil. Post-processing of the examination was performed after image acquisition. The variables used for the study included morphological characteristic pattern on MRI, DWI restrictions, ADC values, and kinetic pattern on dynamic studies. All cases were confirmed with histopathology findings after core biopsy, vacuum-assisted biopsy, surgical excision, mastectomy, or lumpectomy.

Patient positioning: A dedicated double breast surface coil of 18 channels was used, with dimensions of 575×410×205 mm. Patients were positioned prone and dropped both breasts into each of the apertures of the coil. Patients were centered symmetrically over the bilateral breast coil, and the sternum was positioned over the central bar. Compression was not applied, but the breast was softly fixed using foam. Multiplanar localiser was applied with a 3 mm slice thickness, and the Field of View (FOV) was 300-360 mm.

Scanning parameters: MRI sequences obtained included non-enhanced STIR, T2WI, T1WI, DWI, and post-contrast dynamic study. Parameters for MRI sequences were as follows: STIR images (whole breast transverse orientation) with a FOV of 300 mm, TR/TE of 3800/70 ms, a matrix of 448×448, and a slice thickness of 3 mm. STIR images (coronal) with a FOV of 300 mm, TR/TE of 3800/69 ms, a matrix of 384×384, and a slice thickness of 3 mm. T2-weighted images (whole breast transverse orientation) with a FOV of 320 mm, TR/TE of 3000/71, a matrix of 448×448, and a slice thickness of 3 mm. DWI images (whole breast transverse orientation) with a FOV of 360 mm, TR/TE of 6800/70 ms, a matrix of 84×168, and a slice thickness of 3 mm. The b-values used were b1=0 sec/mm^2, b2=800 sec/mm^2, and b3=1500 sec/mm^2. Pre-contrast fat-suppressed T1-weighted images were obtained in whole breast transverse orientation using a 3D Spectral Adiabatic Inversion Recovery (SPAIR) sequence with a FOV of 360 mm, TR/TE of 6.13/3.30 ms, a matrix of 512×512, and a slice thickness of 0.8 mm. The dynamic study post gadolinium T1WI fat sat was obtained in a transverse plane. MultiHance (GdDTPABMA) 0.1 mmoL/kg body weight was injected as a bolus using a pressure injector with a flow rate of 2.0 mL/s, followed by a flush of 20 mL of saline. Post-contrast fat-suppressed T1-weighted images were obtained in whole breast transverse orientation using a 3D SPAIR sequence with a FOV of 320 mm, TR/TE of 4.54/1.73 ms, a matrix of 448×448, and a slice thickness of 1.5 mm. The Flip Angle (FA) was 10 degrees. The dynamic post-contrast study consisted of one pre-contrast T1-weighted FS and five post-contrast series. Postprocessing was performed by digitally subtracting pre-contrast images from the post-contrast MR images.

Maximum Intensity Projection (MIP) of the post-contrast images was also obtained. Kinetic curve analysis was performed using the mean curve technique on the Region of Interest (ROI). The interpretation of the MRI examination was done by analysing the pre-contrast sequences, post-contrast sequences, and post-processing data. The type of post-contrast enhancement was analysed in each lesion (foci enhancement, mass, or non-mass enhancement). The evaluation of enhancement kinetics was defined by detecting the peak percentage of lesion enhancement in the early post-contrast phase (wash-in) and after early phase enhancement (wash-out kinetics). Type-I curve is a persistent, delayed type of enhancement with continuous increased signal intensity throughout the dynamic phase. Type-II curve is like a plateau in which the signal intensity of the lesion has not changed in the delayed phase. Type-III curve shows early uptake and early washout. Apparent diffusion co-efficient calculations were obtained on the workstation by manually drawing ROI.

Image interpretation and analysis: Multiparametric MR imaging data were prospectively evaluated by two radiologists in consensus with more than 15 years of breast imaging and 20 years of MRI experience. All images were transferred to the MAGNETOM Vida syngo software for post-processing. DWI interpretation was done before the DCE-MR interpretation, and both were independent variables. The readers were blinded to histopathology reports as the MRI examinations were performed before the biopsy.

Diffusion Weighted Imaging (DWI) analysis: DWI images were analysed to assess whether the lesion appeared hyperintense and showed corresponding low ADC values. For qualitative analysis, lesions showing diffusion restriction were considered malignant, while those without restriction were considered benign. For quantitative DWI analysis, ADC values were obtained. ADC values were measured on the MAGNETOM Vida syngo software workstation by manually drawing ROI on visibly seen areas of low ADC. Partial volume effects due to normal parenchyma or necrotic tissue were avoided. Mean ADC values were obtained for each lesion and used to plot the ROC curves.

Dynamic Contrast Enhanced MR imaging (DCE-MRI): DCE-MR imaging analysis was performed on the workstation by manually drawing ROI on the most enhanced area of the lesion. Partial volume effects due to adjacent parenchyma in the lesion margins and areas of necrosis detected on morphological and contrast study analysis were avoided when selection the ROI. For DCE-MRI evaluation, all lesions were categorised using the 5th edition of the MRI BIRADS-ACR lexicon. The lesions were categorised as mass or non-mass enhancement categories. Signal intensity on T2-weighted images and the presence or absence of peri-lesional oedema were also observed. For kinetic analysis, the ROI was selected at the enhancing lesions and time signal intensity curves were obtained. Each lesion was analysed in terms of size, shape, margins, enhancement pattern, and kinetic curve pattern. Descriptors according to the American College of Radiology, BI-RADS ACR lexicon were used to differentiate benign and malignant lesions. MRI imaging BIRADS 2 lesions were considered benign, and BIRADS 4 and 5 were considered malignant lesions. BIRADS 3 lesions were considered probably benign lesions. Spiculated and

irregular margins, heterogeneous contrast enhancement, intense early enhancement, and Type-III kinetic curves were the strongest indicators of malignancy in the present study. Criteria to differentiate malignant and benign lesions on MRI were based on morphological and kinetic analysis. After the MRI examination, biopsy of the breast lesion was performed. The final histopathological diagnosis was obtained through core biopsy, surgical excision, mastectomy, or breast-conserving surgeries.

Multiparametric MRI (mpMRI): For combined DCE-MRI, morphology, and DWI analysis, the authors adopted the ACR-BIRADS algorithm to consider a case benign with kinetic curve I or II and morphological features of a benign category with high ADC values. The lesion was considered malignant when it showed low ADC values and morphological features of malignancy according to ACR-BIRADS descriptors with Type-II or III kinetic curves.

STATISTICAL ANALYSIS

MedCalc software bv, Ostend, Belgium, Version 19.4.0, was used for statistical calculations. The authors dichotomised lesions as positive or negative for malignancy for each parameter and used histopathology as the standard of reference. An independent t-test was applied to normally distributed continuous variables to obtain mean, average, and standard deviation values. Pearson's Chi-square tests were applied to non-normally distributed or categorical variables. Mean ADC values for each lesion were kept in continuous form. ROC curves were plotted for the DCE kinetic curve analysis to obtain the area under the curve. DWI results were evaluated in both continuous and binary form. Statistical differences of ROC curves were analysed using the method proposed by DeLong ER et al., [20]. Cut-off values were obtained by maximising the Youden index (sensitivity+specificity-1). Sensitivity, specificity, AUC, and diagnostic accuracy were calculated using the cut-off value of ADC. Diagnostic indexes were calculated for sensitivity, specificity, Positive Predictive Value (PPV), Negative Predictive Values (NPV), and AUC for dynamic CEMR, DWI, and mpMRI. Differences in the area under the curves of multiparametric techniques were obtained using the method proposed by DeLong ER et al., [20].

RESULTS

A total of 254 women with a total of 272 breast lesions were analysed. The mean age was 43.73±13.56 years, with an age range of 18-82 years. Both benign and malignant breast lesions were most common in the 40-49 years of age group in this study, contributing to a total of 80 (31.4%) lesions [Table/Fig-1]. A total of 141 (51.84%) lesions were malignant, and 131 (48.16%) were benign on histopathology. Bilateral lesions were seen in nine cases, and multiple lesions were present in 14 patients. The most common location for breast lesions was the upper outer quadrant, constituting 35.5% (n=98). The most common malignant pathology was invasive ductal carcinoma, constituting 73.7% (n=104), followed by invasive lobular carcinoma in 4% (n=11) out of 141 cases. The most common benign pathology was fibroadenoma, constituting 35.1% (n=46) out of 131 benign lesions [Table/Fig-2].

	Final diagnosis		
Age (Years)	Benign	Malignant	n (%)
18-29	36	7	43 (15.8%)
30-39	48	17	65 (23.9%)
40-49	50	35	85 (31.2%)
50-59	16	18	34 (12.5%)
60-69	12	26	38 (14.0%)
70 Years and above	2	5	7 (2.6%)
Total lesions	164 (60.3%)	108 (39.7%)	272 (100%)

[Table/Fig-1]: Depicting age-wise differentiation and categorisation of lesions.

Malignant lesions	n=141(%)
Ductal invasive carcinoma	104 (38.3)
Invasive lobular carcinoma	11 (4.0)
DCIS	9 (3.3)
Mucinous carcinoma	2 (0.7)
Papillary carcinoma	5 (1.8)
Malignant phyllodes	4 (1.5)
Angiosarcoma	1 (0.4)
Metastasis	3 (1.1)
Paget's disease of nipple and areola	2 (0.7)
Benign lesion	**n=131**
Fibroadenoma/Fibroadenosis	46 (16.9)
Fibrocystic changes without atypia	14 (5.2)
Sclerosing adenosis	6 (2.2)
Infective pathology/abscess/cyst with inflammation	16 (5.9)
Granulomatous mastitis	12 (4.4)
Benign phyllodes	7 (2.6)
Papilloma/atypical ductal hyperplasia	11 (4.0)
Miscellaneous (fat necrosis, radial scar, PASH)	8 (3)
Epithelial atypia	9 (3.3)
Tubular adenoma, lactating adenoma (one each)	2 (0.7)

[Table/Fig-2]: Detailed histopathological diagnosis of the malignant and benign lesions (Total lesions=272).

The most common location for breast lesions in the present study was the upper outer quadrant, constituting 107 (39.33%) cases, followed by involvement of more than one quadrant in 21.69% (n=59) of cases, the upper inner quadrant in 12.5% (n=34) of cases, the central/12 o'clock location in 8.08% (n=22) of cases, the axillary tail/axilla in 5.8% (n=16) of cases, the lower outer quadrant in 4.77% (n=13) of cases, the lower inner quadrant in 2.94% (n=8) of cases, diffuse involvement of the entire breast in nine cases (3.3%), and involvement of only the nipple areolar complex in four cases (1.47%). The most commonly observed lesion out of the 272 lesions was a mass, which was seen in 84.9% (n=231) of cases. Out of these masses, 105 were benign and 126 were malignant [Table/Fig-3]. Non-mass lesions were observed in 15.1% (n=41) of cases, with 26 being benign and 15 being malignant.

Among the non-mass lesions (n=41), three were non-enhancing lesions, 38 were non-mass enhancing lesions (23 benign and 15 malignant), and three benign lesions were non-enhancing lesions. Enhancement types were described in [Table/Fig-3]. Mass and non-mass lesions were categorised according to the MRI BI-RADS lexicon 5th edition. The largest size of a mass was 106 mm, and the smallest was 5 mm, with a mean size of 27.67 mm (±17.18). The mean size for malignant masses was 30.48 mm (±16.9), and for benign masses, it was 24.30 mm (±16.8) ($p<0.0001$).

On DWI, the mean ADC value was 1.17×10^{-3} mm^2/sec for the total of 272 breast lesions. The highest value was 2.94×10^{-3} mm^2/sec, and the lowest was 0.62×10^{-3} mm^2/sec. The mean ADC in malignant lesions was significantly lower ($0.81\pm0.13\times10^{-3}$ mm^2/sec) compared to the mean ADC for benign lesions ($1.55\pm42\times10^{-3}$ mm^2/sec) ($p<0.0001$) [Table/Fig-4].

On DCE-MRI morphological characteristics, the most frequently seen features in malignant masses were irregular shape, irregular or spiculated margins, and heterogeneous or rim internal enhancement patterns ($p<0.0001$). The most common shape of a mass was irregular, found in 22% of benign masses (n=51) and 46.7% of malignant masses (n=108) [Table/Fig-5]. Irregular margins were found in 16.8% of benign masses (n=39) and 35% of malignant masses (n=81). The most frequent shapes for benign breast lesions were oval or round shape, circumscribed margins, and homogeneous/dark septations as internal enhancement characteristics. A representative

Descriptors	Benign (n=131)	Malignant (n=141)	Total (n=272)	p-value
Laterality (n=272)				p=0.6474
Right	77 (28.3%)	79 (29.1%)	156 (57.4%)	
Left	54 (19.8%)	62 (22.8%)	116 (42.6%)	
Type of lesion (n=272)				**p=0.0342**
Mass	105 (38.6%)	126 (46.3%)	231 (84.9%)	
Non-mass lesion	26 (9.6%)	15 (5.5%)	41 (15.1%)	
Mass size (n=231)				**p<0.0001**
Mean size	24.30 mm (±16.88)	30.48 mm (±16.9)		
Mass shape (n=231)				**p<0.0001**
Oval	46 (19.9%)	9 (3.9%)	55 (23.8%)	
Round	8 (3.5%)	11 (4.7%)	19 (8.2%)	
Irregular	51 (22.1%)	106 (45.9%)	157 (68.0%)	
Mass margin (n=231)				**p<0.0001**
Circumscribed	65 (28.1%)	13 (5.6%)	78 (33.8%)	
Irregular	39 (16.9%)	81 (35.06%)	120 (51.9%)	
Spiculated	1 (0.4%)	32 (13.85%)	33 (14.3%)	
Total	105 (45.5%)	126 (54.4%)	231 (100%)	
Mass internal enhancement pattern (n=231)				**p<0.0001**
Homogeneous	43 (18.6%)	16 (6.9%)	59 (25.5%)	
Heterogeneous	26 (11.3%)	81(35.0%)	107 (46.3%)	
Rim enhancement	17 (7.4%)	26 (11.3%)	43 (18.7%)	
Dark internal septations	19 (8.2%)	3 (1.3%)	22(9.5%)	
Total	105 (45.5%)	126(54.5%)	231(100%)	
Kinetic curve analysis (n=272)				**p<0.0001**
Type-I	75 (27.5%)	1(0.36%)	76(27.9%)	
Type-II	53 (19.4%)	24 (8.8%)	77(28.3%)	
Type-III	3 (1.1%)	116(42.6%)	119(43.7%)	
Total	131 (48.2%)	141(51.8%)	272(100%)	
Non-mass distribution (n=41)				p=0.1210
Non-enhancing lesion	3 (7.3%)	0(0%)	3 (7.3%)	
Focal	8 (19.5%)	3 (7.3%)	11 (26.8%)	
Regional	6 (14.6%)	4 (9.8%)	10 (24.4%)	
Segmental	0 (%)	3 (7.3%)	3 (7.3%)	
Diffuse	9 (22.0%)	5 (12.2%)	14 (34.2%)	
Non-mass enhancement (n=41)				p=0.1136
Non-enhancing lesion	3 (7.3%)	0 (%)	3 (7.3%)	
Homogeneous	3 (7.3%)	0 (%)	3 (7.3%)	
Heterogeneous	11 (26.8)	12 (29.3%)	23 (56.1%)	
Clumped	4 (9.8%)	2 (4.8%)	6 (14.6%)	
Clustered ring	5 (12.2%)	1 (2.4%)	6 (14.6%)	
DWI analysis (n=272)				**p<0.0001**
Mean ADC values	1.55±42×10^{-3} mm^2 sec	0.81±0.13×10^{-3} mm^2/sec	1.17×10^{-3} mm^2/sec	
Area under ROC curve (AUC)	0.985 (p<0.001)			
ADC cut-off value	0.987×10 -3 mm^2/sec			

[Table/Fig-3]: Distribution of MRI analysis, dynamic CEMR, qualitative and quantitative variables of Diffusion Weighted Imaging (DWI) for benign and malignant lesions.

case of fibroadenoma showed an oval shape, circumscribed margins, non-enhancing septae, high ADC values of 1.638×10^{-3} mm^2/sec, and a Type-II kinetic curve [Table/Fig-6].

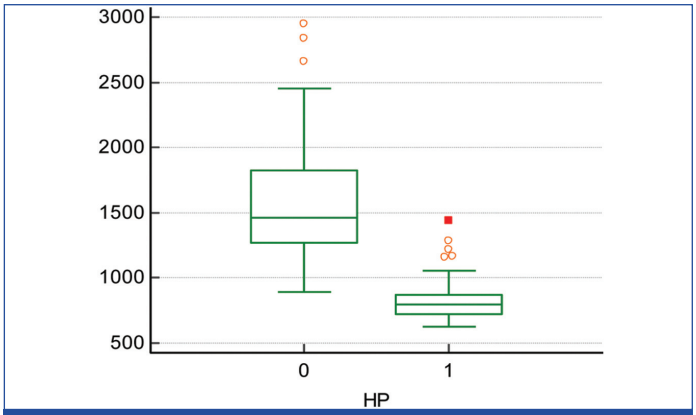

[Table/Fig-4]: Box and whisker plot showed relation between the ADC values of benign (0) and malignant (1) lesions.
0=Benign; 1=Malignant

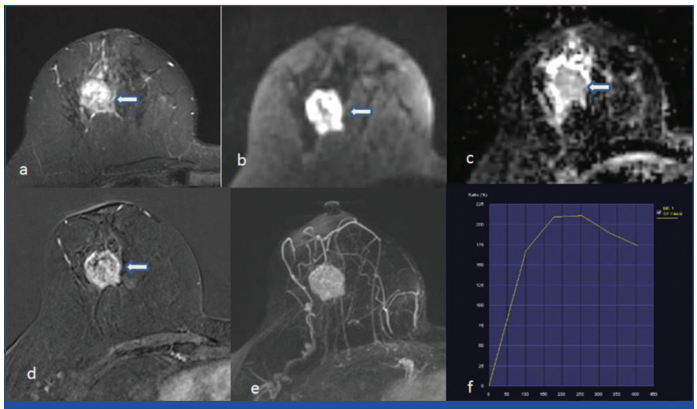

[Table/Fig-5]: Case of Invasive ductal carcinoma: a) Axial STIR MRI image showing heterogeneous mixed signal intensity mass (white arrow); b) Axial DWI MRI showing restriction of malignant mass with; c) low ADC (white arrow); d) Axial fat suppressed DCE-MRI image showing irregular mass with irregular margins and early wash out s/o malignant mass (white arrow); e) MIP of post-contrast dynamic CEMR; f) Type-III kinetic curve.

Non-mass lesions were characterised by regional/segmental/linear/focal distribution and heterogeneous, diffuse, linear, or clumped enhancement. Type-I curve was seen in a total of 76 (27.9%) lesions, Type-II in 77 (28.3%) lesions, and Type-III curve was observed in 119 (43.7%) lesions. Out of all the malignant lesions, 116 (%) lesions demonstrated a Type-III curve, 24 (%) showed a Type-II curve, whereas only 1 (%) lesion demonstrated a Type-I curve (p<0.0001). DCE-MRI showed a sensitivity of 97.87 (95% CI=93.90, 99.55), specificity of 80.15% (95% CI=72.28, 86.60), an AUC of 0.890, and a diagnostic accuracy of 89%. Diffusion-weighted MRI showed a

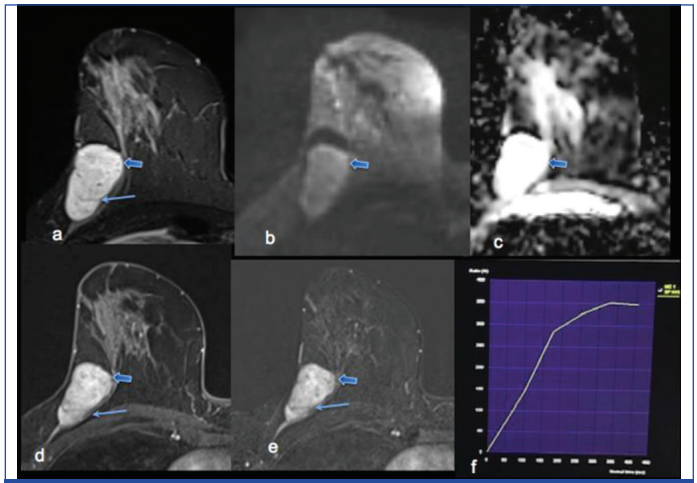

[Table/Fig-6]: MRI in the case of fibroadenoma in right breast of 34-year-old woman: a) STIR axial MRI image showed an oval mass with circumscribed margins (short arrow),which multiple septae (long arrow); b&c) Axial DWI (b value 1500 s/mm^2) showed lesion with corresponding high ADC; c) values of 1.638x10-3 mm^2/sec; d) Axial T1WI DCE non-subtracted; and e) subtracted image showed heterogeneous enhancement of the mass (short arrow) with dark unenhanced septae (long arrow); f) Mass lesion showed Type-II kinetic curve.

sensitivity of 97.16% (95% CI=92.89, 99.22), specificity of 87.02% (95% CI=80.03, 92.25), an AUC of 0.921, and a diagnostic accuracy of 92.27% [Table/Fig-7].

Result	DCE-MRI	DWI	Multiparametric MRI
Sensitivity (%)	97.87 (93.90 to 99.55)	97.16 (92.89 to 99.22)	98.58 (94.97 to 99.82)
Specificity (%)	80.15 (72.28 to 86.60)	87.02 (80.03to 92.25)	93.13 (87.35 to 96.81)
PPV (%)	84.14 (78.98 to 88.22)	88.96 (83.78 to 92.62)	93.91 (89.15 to 96.66)
NPV (%)	97.22 (91.92 to 99.07)	96.61 (91.54 to 98.68)	98.38 (93.90 to 99.58)
Diagnostic accuracy	89.33 (85.04 to 92.74)	92.27 (88.44 to 95.15)	95.95 (92.87 to 97.96)
AUC	0.890 (0.847 to 0.925)	0.921 (0.882 to 0.950)	0.959 (0.928 to 0.979)

[Table/Fig-7]: Diagnostic performances of DCE-MRI, DWI and Multiparametric MRI (mpMRI).

The sensitivity based on ADC values with the optimal criterion of ≤987 was 92.9%, and the specificity was 97.7%. The area under the ROC curve was 0.985, which was statistically significant (p<0.001) [Table/Fig-8]. The multiparametric study revealed a sensitivity of 98.58% (95% CI=94.97, 99.82), specificity of 93.13% (95% CI=87.35, 96.81), an AUC of 0.959, and a diagnostic accuracy of 95.95%. Pairwise comparisons of the Area Under Curve (AUC) of ROC curves were obtained and shown in [Table/Fig-8,9]. There were significant differences in the areas between DCE-Mp MRI (p=0.0001), but the difference was not significant between DCE-MRI and DWI ROC curves (p=0.1076) [Table/Fig-8,10].

Variable	AUC	SE	95% CI
DCE-MRI	0.890	0.0185	0.847 to 0.925
DWI	0.921	0.0163	0.882 to 0.950
ADC	0.985	0.00531	0.963 to 0.996
CEMR (semi-quantitative)	0.947	0.0116	0.914 to 0.971
mP MRI	0.959	0.0122	0.928 to 0.979
DCE-MRI ~ DWI			
Difference between areas		0.0308	
Standard error[a]		0.0191	
95% Confidence interval		-0.00672 to 0.0683	
Significance level		p=0.1076	
DCE-MRI ~ MpMRI			
Difference between areas		0.0684	
Standard error[a]		0.0152	
95% Confidence interval		0.0387 to 0.0981	
Significance level		**p=0.0001**	
DWI ~ mPMRI			
Difference between areas		0.0376	
Standard error[a]		0.0167	
95% Confidence interval		0.00808 to 0.0753	
Significance level		**p=0.0240**	

[Table/Fig-8]: Pairwise comparison of ROC curves.
[a]DeLong ER et al., 1988
[b]Binomial exact

DISCUSSION

Multiparametric MRI has the potential to provide morphological as well as functional information about breast tumours, which can further improve diagnostic accuracy [12,14,15]. In this study, we analysed individual ACR-BIRADS descriptors for DCE-MRI and qualitative and quantitative variables from DWI and their combined results for diagnostic accuracy. The authors analysed the DCE-MRI characteristics of each mass lesion, including shape, margin, internal

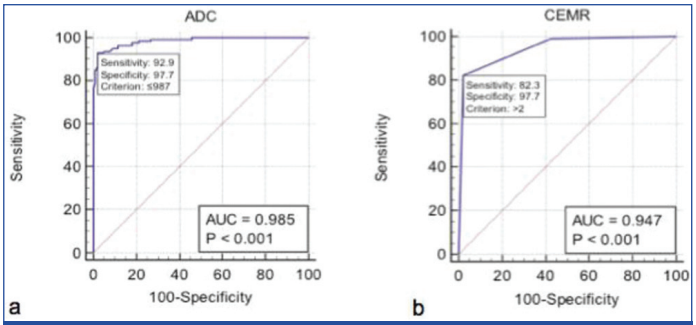

[Table/Fig-9]: ROC curves of quantitative variables of DWI and CEMR: a) ROC curve of ADC values showed area under the curve of 0.985; b) ROC curve of kinetic curves obtained on dynamic CEMR showed area under the curve of 0.947.
[a]DeLong ER et al., 1988
[b]Binomial exact

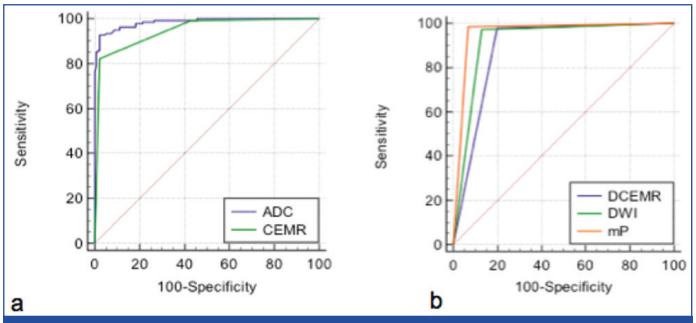

[Table/Fig-10]: Comparative ROC for various parameters: a) Comparative ROC curves for the quantitative analysis of the ADC values and CEMR kinetic curves; b) ROC curves illustrate higher diagnostic values (higher sensitivity, specificity and larger area under the curve) of multiparametric MRI (mpMRI).

enhancement pattern, and enhancement kinetics. The authors also observed the ADC values as a quantitative measure and DWI signal intensity as a qualitative measure of DWI. The present study found that lesions with irregular or spiculated margins and low ADC values are more likely to be malignant. The most common shapes and margins were irregular in malignant lesions. Type-III kinetic curve was the most common in malignant lesions, while Type-I kinetic curve was more common in benign lesions. Multiparametric MRI increased the diagnostic accuracy with an area under the curve of 0.959, while the area under the curve for DCE-MRI was 0.890 and for DWI was 0.921, respectively.

The most common location for breast lesions was the upper outer quadrant, which constituted 107 (39.33%) cases. Studies have mentioned that the upper outer quadrant is the most common location for malignant as well as benign lesions, possibly due to the large amount of glandular tissue present in that area [11,14,21]. This study included a mixed population of rural and urban women, some of whom presented with large tumours. In the present study, 15.1% (n=41) of the lesions were non-mass lesions, out of which 9.6% (n=26) lesions were benign. Granulomatous mastitis and other chronic infective pathologies can show features that are indistinguishable from malignant pathology [22]. These pathologies are more common in Asian countries, so the study population is different from most published data. Most of the malignant masses in the present study were irregular in shape, while most of the benign masses showed an oval or round shape. Wedegartner et al., [23] and Tozaki M et al., [24] also showed in their study that most of the benign lesions were oval or round shaped, while malignant masses had an irregular shape. This is consistent with previous studies [10,12,14,25,26]. In the present study, the authors found that spiculated or irregular lesions with initial fast or medium contrast enhancement and lower ADC values are more likely to be malignant. Furthermore, combining DWI with ADC mapping with DCE-MRI improved the diagnostic accuracy, as earlier authors have reported [7-9].

In the present study, the mean ADC in the malignant lesions was significantly lower ($0.81\pm0.13\times10^{-3}$ mm^2/sec) than the mean ADC

values for benign lesions (1.55±42×10^{-3} mm^2/sec). The area under the curve for ADC values in this study was 0.985 (p<0.001) with a cut-off value of 0.987×10^{-3} mm^2/sec to achieve a sensitivity of 92.91% and specificity of 97.71%. Hetta W [19] observed that the malignant lesions demonstrated a mean ADC value of 1.03±0.35, whereas benign lesions demonstrated a mean ADC value of 1.38±0.26. In their study, DCE-MRI showed 80% sensitivity and a specificity of 73.33%, whereas in the present study, DCE-MRI showed 97.87% sensitivity and 80.15% specificity. Yadav P and Chauhan S reported that combined DWI and DCE-MRI showed a sensitivity of 95% and specificity of 96.43% [14]. The mean ADC of the malignant lesions was 1.014 and of benign lesions was 1.905 in their study. El Bakry MAH et al., [26] found that DCE-MRI showed a sensitivity of 91.7%, specificity of 84.2%, PPV of 84.6%, and NPV of about 91.4%. In their study, the mean ADC value of benign lesions was 2.05 and of malignant lesions was 0.92, with a cut-off value of ADC of 1.32.

Wedegartner U et al., [23] observed in a meta-analysis of the diagnostic performance of quantitative diffusion-weighted MR imaging in breast lesions that mean ADC values of the malignant lesions ranged from 0.87 to 1.36×10^{-3} mm^2/s, and of benign lesions ranged from 1.00 to 1.82×10^{-3} mm^2/s. Cut-off values differentiating benign and malignant lesions ranged from 0.90 to 1.76×10^{-3} mm^2/s, while the sensitivity and specificity ranged from 63% to 100% and 46% to 97%, respectively. Various authors have proposed different ADC cut-off values to differentiate malignant from benign lesions [14,19,25]. Pinker K et al., [27] conducted a study to develop a combined contrast-enhanced MRI and diffusion-weighted MRI adapted for BI-RADS for mpMRI of the breast and observed that multiparametric 3-T MRI of the breast significantly improves the diagnostic accuracy. They concluded that multiparametric MRI with three parameters, DCE, DWI, and MRS, showed the highest sensitivity of 100% and a PPV of 93.7%.

Zhang M et al., [8] conducted a study to develop an mpMRI model for breast cancer diagnosis. They incorporated ACR-BIRADS recommended descriptors for breast MRI. They concluded that mpMRI with DCE-MRI and DWI with ADC mapping improves the diagnosis of breast cancers. In their model, using quantitative and qualitative descriptors from DCE-MRI and DWI significantly improves the diagnostic accuracy of breast MRI. In the present study, the authors also used qualitative and quantitative descriptors from DCE-MRI and DWI with ADC mapping to improve the diagnostic accuracy.

Various studies have been performed to assess the role of an MR imaging protocol that combines DCE-MRI and DWI in patients with suspicious breast lesions [17,26-28]. In this study, mpMRI with DCE-MR and DWI parameters showed 98.58% sensitivity and 93.13% specificity, with an improved diagnostic accuracy of 95.95% and an AUC of 0.959. The results of the present study suggest that by combining these methods, the detection of false positive cases decreases significantly.

DWI has the potential to be used along with DCE-MRI to obtain good diagnostic accuracy, and ADC values can be used to evaluate the prognosis and therapeutic outcome. It can be used to differentiate high-grade breast cancer from low-grade breast tumours and assess the response to neoadjuvant chemotherapy [7,28-30]. DWI characteristics can also be used as guidance for MRI biopsy to target the most aggressive part of the lesion and reduce sampling error.

However, even with mpMRI, lesions with atypia and high cellular lesions like tubular and lactating adenomas showed false positive results in this study. Abscesses also showed false positive results with diffusion restriction. High-risk lesions like atypical ductal hyperplasia, epithelial hyperplasia with atypia, and sclerosing adenosis also showed false positive results [29,31]. Other false positive lesions were chronic abscesses and infective lesions, which showed low ADC values on DWI and highly suspicious features on DCE-MRI [32].

Recently published studies have focused on the utility of a high b value of 1500, and they concluded that there is better cancer detection with the high b value [16]. Recently published studies on the feasibility of synthetic DWI MRI have shown that qualitative analysis of the lesion is better with the use of a high b-value of 1500 [16].

Limitation(s)

The study had a small number of pure Ductal Carcinoma In Situ (DCIS) cases and invasive lobular carcinoma subgroups. Another limitation is that this study was conducted in a single tertiary care institution. The DWI images were obtained at b-values of 800 and 1500; however, the diagnostic performance of the b-value 800 was not included in the study, as the purpose was to evaluate the diagnostic performance of the high b-value.

CONCLUSION(S)

The mpMRI, utilising qualitative and quantitative descriptors from DCE-MRI and DWI with a high b-value, improves diagnostic accuracy and reduces false positive cases. High-resolution DWI, using the RESOLVE technique, has less distortion and shows good sensitivity in detection malignant lesions. Based on this study, the authors propose an mpMRI protocol to obtain better diagnostic accuracy, which has the potential to reduce unnecessary biopsies.

REFERENCES

[1] Jemal A, Bray F, Melissa MC, Jacques F, Elizabeth W, Forman D. Global cancer statistics. CA Cancer J Clin. 2011;61(2):69-90.

[2] Morris EA, Comstock CE, Lee CH. ACR BI-RADS® Magnetic Resonance Imaging. In: ACR BI-RADS® Atlas, Breast Imaging Reporting and Data System. Reston, VA, American College of Radiology; 2013. https://www.scirp.org/reference/referencespapers?referenceid=2190244.

[3] Kuhl CK, Strobel K, Bieling H, Leutner C, Schild HH, Schrading S. Supplemental breast MR imaging screening of women with average risk of breast cancer. Radiology. 2017;283(2):361-70.

[4] Krammer J, Pinker-Domenig K, Robson ME, Gönen M, Bernard-Davila B, Morris EA, et al. Breast cancer detection and tumour characteristics in BRCA1 and BRCA2 mutation carriers. Breast Cancer Res Treat. 2017;163(3):565-71.

[5] Paran Y, Bendel P, Margalit R, Degani H. Water diffusion in the different microenvironments of breast cancer. NMR Biomed. 2004;17(4):170-80.

[6] Rubesova E, Grell AS, De Maertelaer V, Metens T, Chao SL, Lemort M. Quantitative diffusion imaging in breast cancer: A clinical prospective study. J Magn Reson Imaging. 2006;24(2):319-24.

[7] Partridge SC, McDonald ES. Diffusion weighted magnetic resonance imaging of the breast: Protocol optimization, interpretation, and clinical applications. Magn Reson Imaging Clin N Am. 2013;21(3):601-24.

[8] Zhang M, Horvat VJ, Bernard-Davila MPH, Adele M, Leithner D, Albiztegui R, et al. Multiparametric MRI model with dynamic contrast enhanced and diffusion weighted imaging enables breast cancer diagnosis with high accuracy. J Magn Reson Imaging. 2019;49(3):864-74.

[9] Pinker K, Baltzer P, Bogner W, Leithner D, Trattnig S, Zaric O, et al. Multiparametric MR imaging with high-resolution dynamic contrast-enhanced and diffusion-weighted imaging at 7 T improves the assessment breast tumours: A feasibility study. Radiology. 2015;2015:276(2):141905.

[10] Yabuuchi H, Matsuo Y, Kamitani T, Setoguchi T, Okafuji T, Soeda H, et al. Non-mass-like enhancement on contrast-enhanced breast MR imaging: Lesion characterization using combination of dynamic contrast enhanced and diffusion-weighted MR images. Eur J Radiol. 2010;75(1):e126-32.

[11] Yabuuchi H, Matsuo Y, Okafuji T, Kamitani T, Soeda H, Setoguchi T, et al. Enhanced mass on contrast-enhanced breast MR imaging: Lesion characterization using combination of dynamic contrast-enhanced and diffusion-weighted MR images. J Magn Reson Imaging. 2008;28(5):1157-65.

[12] Schmitz AM, Veldhuis WB, Menke-Pluijmers MB, van der Kemp WJ, van der Velden TA, Kock MC, et al. Multipara- metric MRI with dynamic contrast enhancement, diffusion-weighted imaging, and 31-phosphorus spectroscopy at 7T for characterization of breast cancer. Invest Radiol. 2015;50(11):766-71.

[13] Kul S, Cansu A, Alhan E, Dinc H, Gunes G, Reis A. Contribution of diffusion-weighted imaging to dynamic contrast enhanced MRI in the characterization of breast tumours. AJR Am J Roentgenol. 2011;196(1):210-17.

[14] Yadav P, Chauhan S. Effectivity of combined diffusion-weighted imaging and contrast-enhanced MRI in malignant and benign breast lesions. Pol J Radiol. 2018:83:e82-93. Doi: 10.5114/pjr.2018.74363. eCollection 2018.

[15] Bogner W, Pinker-Domenig K, Bickel H, Chmelik M, Weber M, Helbich TH, et al. Readout-segemnted echo-planar imaging improves the diagnostic performance of diffusion weighted MR breast examinations at 3.0 T. Radiology. 2012;263(1):64-76.

[16] Park JH, Yun B, Jang M, Ahn HS, Kim SM, Lee SH, et al. Comparison of the diagnostic performance of synthetic versus acquired high b-value (1500 s/mm2) diffusion-weighted MRI in women with breast cancers. J Magn Reson Imaging. 2019;49(3):857-63.
[17] Yadav P, Harit S, Kumar D. Efficacy of high-resolution, 3-D diffusion-weighted imaging in the detection of breast cancer compared to dynamic contrast-enhanced magnetic resonance imaging. Pol J Radiol. 2021;86:e277-86. Doi: 10.5114/pjr.2021.106207. PMID: 34136045; PMCID: PMC8186310.
[18] Zhou J, Chen E, Xu H, Ye Q, Li J, Ye S, et al. Feasibility and diagnostic performance of voxelwise computed diffusion-weighted imaging in breast cancer. J Magn Reson Imaging. 2019;49(6):1610-16.
[19] Hetta W. Role of diffusion weighted images combined with breast MRI in improving the detection and differentiation of breast lesions. Egyptian J Radiol Nucl Med. 2015;46(1):259-70.
[20] DeLong ER, DeLong DM, Clarke-Pearson DL. Comparing the areas under two or more correlated receiver operating characteristic curves: A nonparametric approach. Biometrics. 1988;44(3):837-45.
[21] Darbre DPH. Recorded quadrant incidence of female breast cancer in Great Britain suggests a disproportionate increase in the upper outer quadrant of the breast. Anti-Cancer Res. 2005;25(3C):2543-50.
[22] Tewari M, Shukla HS. Breast tuberculosis: Diagnosis, clinical features and management. Indian J Med Res. 2005;122(2):103-10.
[23] Wedegartner U, Bick U, Wörtler K, Rummeny E, Bongartz G. Differentiation between benign and malignant findings on MR- mammography: Usefulness of morphological criteria. Eur Radiol. 2001;11(9):1645-50.
[24] Tozaki M, Igarashi T, Fukuda K. Positive and negative predictive values of BI-RADS descriptors for focal breast masses. Magn Reson Med Sci. 2006;5(1):07-15.
[25] Chen X, Li W, Zhang Y, Wu Q, Guo Y, Bai Z. Meta-analysis of quantitative diffusion-weighted MR imaging in the differential diagnosis of breast lesions. BMC Cancer. 2010;10:693. https://www.ncbi.nlm.nih.gov/books/NBK79058/.
[26] El Bakry MAH, Sultan AA, El-Tokhy NAE, Yossif TF, Ali CAA. Role of diffusion weighted imaging and dynamic contrast enhanced magnetic resonance imaging in breast tumours. Egypt J Radiol Nucl Med. 2015;46(3):791-804.
[27] Pinker K, Bickel H, Helbich TH, Gruber S, Dubsky P, Pluschnig U, et al. Combined contrast-enhanced magnetic resonance and diffusion-weighted imaging reading adapted to the "Breast Imaging Reporting and Data System" for multiparametric 3-T imaging of breast lesions. Eur Radiol. 2013;23(7):1791-802.
[28] Zhang L, Tang M, Min Z, Lu J, Lei X, Zhang X. Accuracy of combined dynamic contrast-enhanced magnetic resonance imaging and diffusion-weighted imaging for breast cancer detection: A meta-analysis. Acta Radiol. 2016;57(6):651-60.
[29] Akin Y, Ugurlu MU, Kaya H, Aribal E. Diagnostic value of diffusion weighted imaging and apparent diffusion coefficient values in the differentiation of breast lesions, histpathologic subgroups and correlation with prognostic factors using 3.0 Tesla MR. J Breast Health. 2016;12(3):123-32.
[30] Bae MS, Shin SU, Ryu HS, Han W, Im SA, Park IA, et al. Pretreatment MR imaging features of triple-negative breast cancer: Association with response to neoadjuvant chemotherapy and recurrence-free survival. Radiology. 2016;281(2):392-400.
[31] Bianchi S, Caini S, Renne G, Cassano E, Ambrogetti D, Cattani MG, et al. Positive predictive value for malignancy on surgical excision of breast lesions of uncertain malignant potential (B3) diagnosed by stereotactic vacuum-assisted needle core biopsy (VANCB): A large multiinstitutional study in Italy. Breast. 2011;20(3):264-70.
[32] Unal O, Koparan HI, Avcu S, Kalender AM, Kisli E. The diagnostic value of diffusion-weighted magnetic resonance imaging in soft tissue abscesses. Eur J Radiol. 2011;77(3):490-94.

PARTICULARS OF CONTRIBUTORS:
1. Professor, Department of Radiology and Imaging, Head; Interventional Radiology, Dr. D.Y. Patil Medical College, Hospital and Research Centre, Pimpri, Pune, Dr. D.Y. Patil Vidyapeeth, Pimpri, Pune, Maharashtra, India.
2. Associate Professor, Department of Radiology and Imaging, Dr. D.Y. Patil Medical College, Hospital and Research Centre, Pimpri, Pune, Dr. D.Y. Patil Vidyapeeth, Pimpri, Pune, Maharashtra, India.
3. Research Assistant, Dr. D.Y. Patil Medical College, Hospital and Research Centre, Pimpri, Pune, Dr. D.Y. Patil Vidyapeeth, Pimpri, Pune, Maharashtra, India.

NAME, ADDRESS, E-MAIL ID OF THE CORRESPONDING AUTHOR:
Dr. Pratiksha Yadav,
Professor, Department of Radiology and Imaging, Dr. D.Y. Patil Medical College, Hospital and Research Centre, Dr. D.Y. Patil Vidyapeeth, Pimpri,
Pune-411018, Maharashtra, India.
E-mail: yadavpratiksha@hotmail.com

PLAGIARISM CHECKING METHODS: [Jain H et al.]
- Plagiarism X-checker: Nov 10, 2023
- Manual Googling: Dec 02, 2023
- iThenticate Software: Dec 11, 2023 (14%)

ETYMOLOGY: Author Origin

EMENDATIONS: 6

AUTHOR DECLARATION:
- Financial or Other Competing Interests: The research was supported by the Institution (DPU), which waived off MRI investigation charges.
- Was Ethics Committee Approval obtained for this study? Yes
- Was informed consent obtained from the subjects involved in the study? Yes
- For any images presented appropriate consent has been obtained from the subjects. Yes

Date of Submission: **Nov 04, 2023**
Date of Peer Review: **Dec 01, 2023**
Date of Acceptance: **Dec 12, 2023**
Date of Publishing: **Jan 01, 2024**